J Nanostruct 16(2): 2097-2114, Spring 2026

RESEARCH PAPER

Analytical Investigation of the Adsorption Behavior of Eriochrome Black T and Crystal Violet Dyes onto a Fe_3O_4/CuO/ Activated Carbon Nanocomposite in Aqueous Solution

Nisreen AbdulKareem Abdulaali [1], *Noor Sabah khadim* [2], *Zainab Hussain* [1] *

[1] *Department of Chemistry, College of Science, University of Misan, Maysan, Iraq*

[2] *Department of Pharmaceutical Chemistry, College of Pharmacy, University of Misan, Maysan, Iraq*

ARTICLE INFO

Article History:
Received 13 December 2025
Accepted 20 March 2026
Published 01 April 2026

Keywords:
Composite
Crystal violet
Eriochrome black T
Peel kiwi
Peel peach

ABSTRACT

The outcomes from this research indicated that utilizing activated carbon derived from kiwi and peach peels on the surface of a Fe_3O_4-CuO (iron oxide/copper oxide) nanocomposite increases its surface properties, including its adsorption capability due to the high porosity and functional groups associated with the carbon. This results in additional active sites that can adsorb contaminants to the carbon surface. The carbon/metallic phase synergistic effect enhances the surface reactivity of the iron oxide and copper nanoparticles as shown by the x-ray diffraction analysis (XRD), which shows evidence of crystalline phase formation for all the oxide nanoparticles, along with the Fourier transform infrared spectroscopy (FTIR) analysis indicating the presence of functional groups and increasing number of active sites available for adsorption of contaminants. The Brunauer–Emmett–Teller (BET) analysis of these nanomaterials indicates that they possess high surface areas and excellent porosities, while the zeta potential values confirm that the nanocomposite has stable surface charges. Scanning electron microscopy and energy dispersive X-ray spectroscopy have also been used to establish consistency in elemental (carbon, oxygen, copper, and iron) distributions on the surface of these nanomaterials correlating to enhanced overall adsorption and removal efficiencies of contaminants. Adsorption involves a combination of equivalent and distinct site types on a surface, as supported by the Langmuir and Freundlich data; the magnetic attributes of the compound make it easily separable/able to be reused, and therefore can function as an efficient, promising material for use in treating water.

How to cite this article
AbdulKareem Abdulaali N, Sabah khadim N, Hussain Z. Analytical Investigation of the Adsorption Behavior of Eriochrome Black T and Crystal Violet Dyes onto a Fe_3O_4/CuO/Activated Carbon Nanocomposite in Aqueous Solution. J Nanostruct, 2026; 16(2):2097-2114. DOI: 10.22052/JNS.2026.02.056

INTRODUCTION

Urbanization can be viewed as a result of industrialization. As mentioned, industrialization can bring many positive benefits, but it has also brought many negative side effects to the natural ecosystems of the planet, as it can put various kinds of pollution into water sources. One of the very serious problems facing every country today is pollution of freshwater resources, which are a renewable resource necessary to support all types

* *Corresponding Author Email: zainab_alaa@ymail.com*

of life [1].

The contamination of wastewater with dyes is a huge environmental problem. This came from many industrial processes, including textile, leather, paper, and dye manufacturers. The wastewater for all of these industries contains various types of synthetic dye, and the dyes may be very brightly coloured and have complex chemical forms. The large-scale release of these dyes into surface waterways results in less beautiful water and poses a serious risk to ecosystems.

Many different techniques exist to remove contaminants from both environmental waters and wastewater. The most common approaches can be classified into biological, chemical, and physical water treatment processes (see Fig. 1) [5]. Among all of these treatment methods, one type is known as the most common, which is referred to as adsorption, the collection of certain molecules (i.e. adsorption) at a gas-solid interface or a liquid-solid interface, this is considered an adsorption phenomenon. [6].

Adsorption is one of the most widely accepted techniques for removing dye from wastewater, as all, basically, they all have advantageous properties such as being efficient, inexpensive, energy-efficient, easily designable and easy to use [8]. Commercial activated carbon has been the preferred adsorbent used in the industry; however, there is continuing research for other cost effective and efficient organic/inorganic alternative sources for adsorbent due to the various high costs associated with producing and regenerating commercial activated carbon [9].

According to [10], nanomaterials make excellent solid-phase adsorbents. Compared with conventional types of adsorbent materials, nanomaterials have some very different characteristics (1) due to their smaller size and larger surface area they will interact more with either other nanomaterials or the analytes of interest, thus they will provide better adsorption/ separation performance than most conventional types of adsorbents [11]. (2) Nanoparticles exhibit excellent surface energy and diffusion rates; all particles will be in total contact with each other, allowing them to reach equilibrium quickly after exposure to a contaminant and providing them with exceptional adsorption characteristics for many types of contaminants - especially metal ions and organic compounds [12]. (3) Nanomaterials are also easy to modify - by changing the surface chemistry of these materials it is possible to create even better-performing adsorbents by producing different types of functional groups that can be used to selectively extract target compounds. Because of these valuable properties, nanomaterials have been utilized extensively throughout the various fields of chemistry as adsorbents [13].

Recently, there has been an increase in the

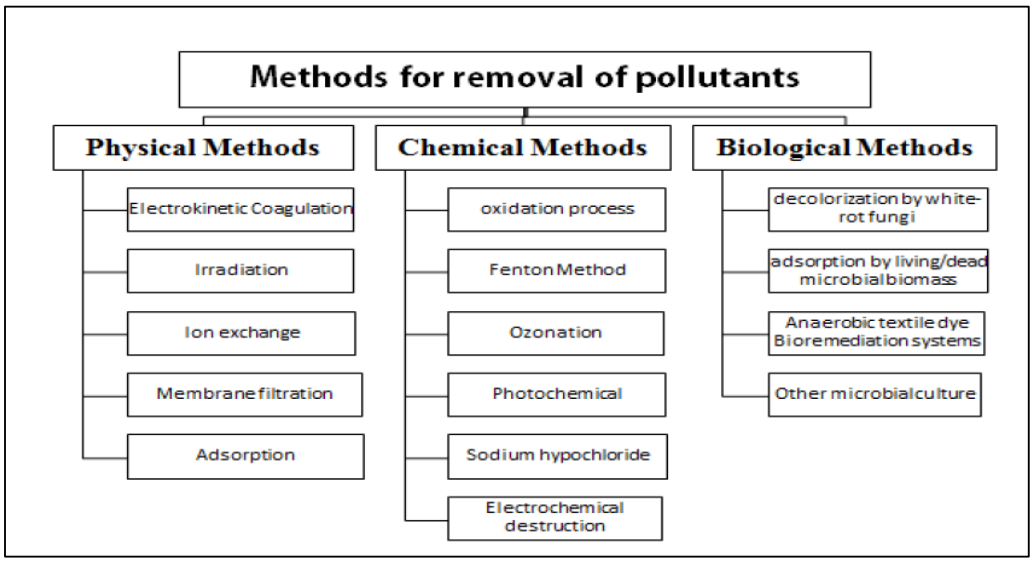

Fig. 1. Diagram of different techniques for dye removal from water followed by adsorption technique. utilization over other water treatment techniques [7].

number of publications where researchers are investigating the possibility of using nanomaterials such as modified silicon and zeolites, as well as the potential benefits of using these types of materials (ZnO and TiO_2 with clay or in combination with other materials I.e., metal-organic frameworks, carbon nanocages, graphene, nanotubes, porous polymers, Fe_3O_4, CuO, functional 3D boron nitride nanostructures) for the removal of dyestuffs from aqueous solutions [14-18]; in fact most of them can be reused and are extremely effective in removing dyestuffs due to their large specific surface area and are therefore quick to do so.

The present study was conducted on the adsorption of two commercially available textile dyes, Crystal Violet & Eriochrome T (Fig. 2), from an aqueous medium onto Fe_3O_4/CuO/Activated Carbon Nanocomposite. The study also provides kinetic modeling and equilibrium isotherm analyses along with primary data for investigating the effects of varying experimental parameters such as initial dye concentration, sorption contact time, temperature and sorbent dosage.

MATERIALS AND METHODS

Materials

Kiwi and peaches collected from the domestic market, Misan, Iraq; Ferric chloride anhydrous (%97 THOMAS BAKER), Sodium hydroxide (%98, THOMAS BAKER), Hydrogen chloride (%37,

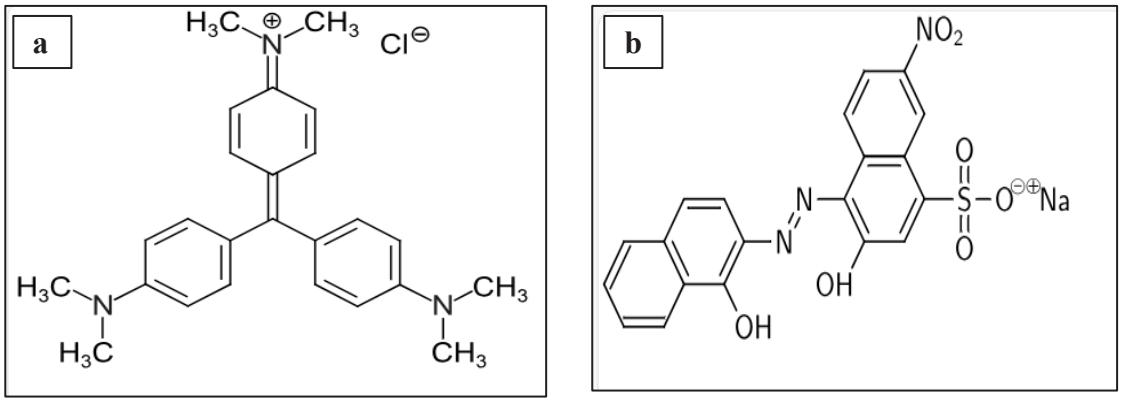

Fig. 2. a) Crystal Violet (CV) dye b) Eriochrome Black T (EBT) dye Chemical Structure [19-20].

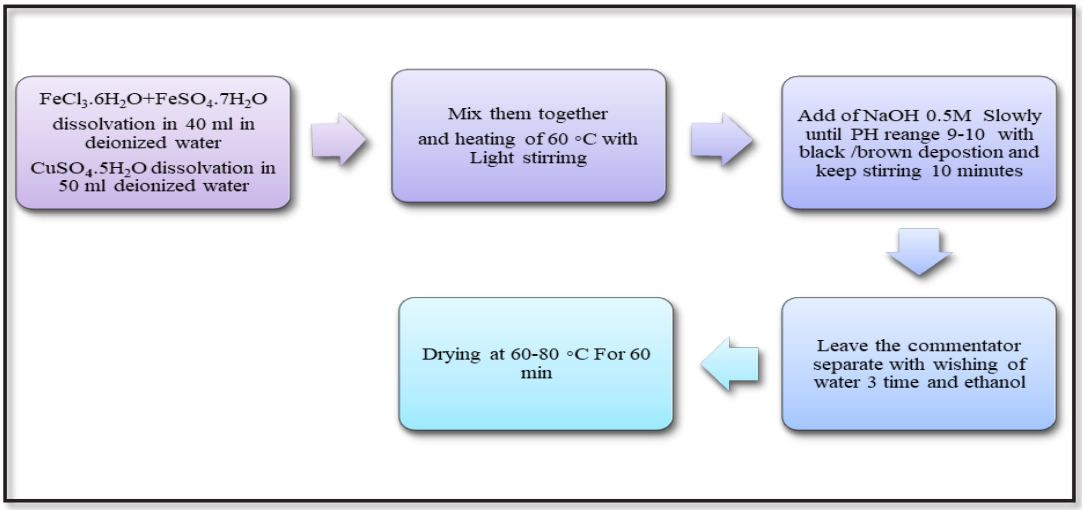

Fig. 3. Flowchart of synthesis technique of magnetic (Fe_3O_4-CuO) nanoparticles.

ROMIL-SA), Hydrated copper (II) Sulfate (%99.9, HI media -India), Ethanol absolute (%99.9, ROMIL-SA), Iron (II) sulfate heptahydrate (%99.9, HI media -India) These materials are highly pure and do not require purification, Creating an ionic solution with deionized water, Polyethylene glycol (%99.9, Sandy croft-UK), Crystal violet (%99.9, HI media -India), Eriochrome Black T(%99, CDH -INDIA).

Preparation of nanocomposite Fe_3O_4-CuO

0.9 g of acetanilide was added to 80 mL of an aqueous solution containing salt that had been made by dissolving 1.67 g of ferric chloride hexahydrate ($FeCl_3 \cdot 6H_2O$) into 50 mL of pure deionized water. Separately, 1.50 g of ferrous sulfate heptahydrate ($FeSO_4 \cdot 7H_2O$) was dissolved into 40 mL of pure deionized water. The two above solutions were combined and heated to 60°C while stirring. One drop at a time, 1 M sodium hydroxide (NaOH) was added to the mixture until the pH of the mixture was between 9 and 10. The mixture was stirred for an additional fifteen minutes. The black precipitate created from the above reactions was filtered from the reaction mixture by using a magnetic bar and an external magnetic field as described previously [21]. After the filtered solution had been cleaned repeatedly by using both deionized and ethanol, the cleaned precipitate was allowed to settle to room temperature for 10 minutes. The wet precipitate then underwent a drying process in an oven at 60 °C for 1 hour. A diagram of the entire procedure is shown Fig. 3.

Preparation of Activated carbon from kiwi and peach peels

Kiwi and peach skins are harvested, then hand washed to remove dirt before being left uncovered outside under direct sunlight for 1-2 weeks for total drying. They will then be cut into small pieces, then ground into fine granules. In an acid resistant glass container, 10g of the peel will be mixed with 12ml of phosphoric acid (85% H_3PO_4) and enough water (50-100ml) to cover the mixture. The mixture must be stirred for a period of 2-4 hours at room temperature to thoroughly combine, and then left to sit overnight to allow for maximum absorption. After sitting overnight, the solution will be strained, through a 45 micron filter paper to remove excess liquid and then dried in an oven at 105 °C for a period of 2-6 hours. A small heat-resistant crucible is used to put the dried sample in then put a lid on the container to minimize airflow and then put the crucible in a muffle furnace; the temperature is raised 5-10 degrees C/ minute until 450 degrees C for 1 hour. Once the heat source has been turned off, the crucible is allowed to cool to room temperature prior to removal of the

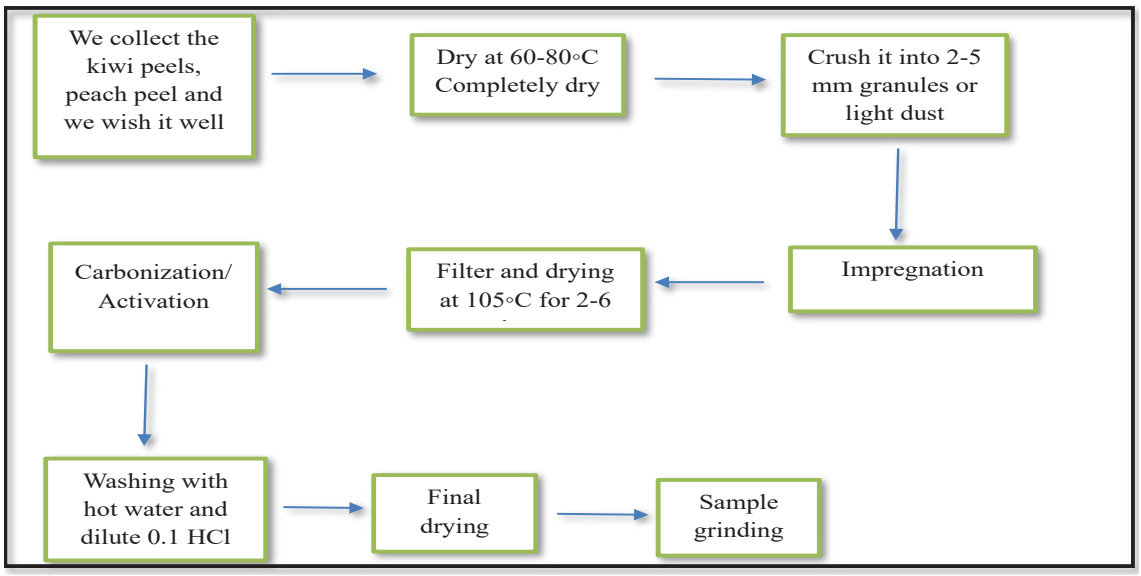

Fig. 4. Flowchart of synthesis Activated Carbon.

sample. The filtered sample is washed first with hot water to remove any phosphate residues and retested for pH, second by using a dilute acid wash (0.1M HCl), and third with hot water until the pH is neutral. The dried product is then dried at 105°C for 3-6 hours., Fig. 4.

Preparation of Fe_3O_4-CuO nanoparticle grafted on carbon activated

To create activated carbon (AC) loaded with iron oxide (Fe_3O_4) and copper oxide (CuO), the following methods should be used. Start by dissolving 0.5 g of activated carbon in 80-100 ml of deionized water using sonication for 3-5 minutes and stir to mix thoroughly. Dissolve 1.0 g of Fe_3O_4 (CuO) powder, made according to the previous instructions, in 70 ml of deionized water and blend together, then gradually add this solution to the activated carbon suspension while stirring, using a sonicator for 15-30 minutes to assist with full dispersion. The resulting product will be then separated by filtration through filter paper, washed 2 times with water and once with ethanol for salt removal. The product is dried in an oven at 60 to 80 degree Celsius (C), over a period of 30 to 60 minute, producing AC loaded Fe_3O_4/CuO [23], show in the Fig. 5.

Characterization method

The tools employed in the experimental studies consisted of Laboratory Oven (WR-20, Co, Ltd. China), Sensitive electronic balance (, WORNER LAB‹China), Hot plate with Magnetic stirrer (MSH-420, BOSCO, Germany), Muffle furnace (CWF1200, CARBOLTE, UK), Bath sonicator (WHC-A10H, Daihan Scientific‹ China), UV Spectrophotometer (1800, SHIMADZU, Japan),X- ray diffraction (Philips xpert PA analytical Holland, Iran) used for studying of Fe_3O_4-CuO NPs,Fe_3O_4-CuO-Ac , Scanning electron microscopy (Sem) (TESCAN MIRA3 FRENCH, Iran) under an accelerating voltage 15 kv, Zeta potential)Dynamic Light Scattering,SZ-100,Japan).

RESULTS AND DISCUSSION

FT-IR spectroscopy

FTIR spectroscopy examined the functional chemical groups of the synthesized Fe_3O_4 and CuO nanoparticles in the 400-4000 cm-1 range. Fig. 6 depicts six main peaks typical of the nanoparticles: 3394 cm^{-1}, 1620 cm^{-1}, 1553 cm^{-1}, 1492 cm^{-1}, 1340 cm^{-1}, and 1070 cm^{-1}. These peaks correspond with the following vibrations: O-H hydroxyl group in alcohol, C-O from primary alcohols; C=O from alkenes, C-N, and =C–H groups. Conversely, the band between 400-500 cm^{-1} corresponds with our Fe_3O_4 and CuO nanoparticles' Fe–O/Cu–O stretching vibrations [25]. In addition, the FTIR (Fig. 4) for the Ac kiwi peel sample shows one extended O-H band at 3455 cm^{-1}; this band is ubiquitous among many plant peels, and the weak bands at 1250-1049 cm-1 indicate

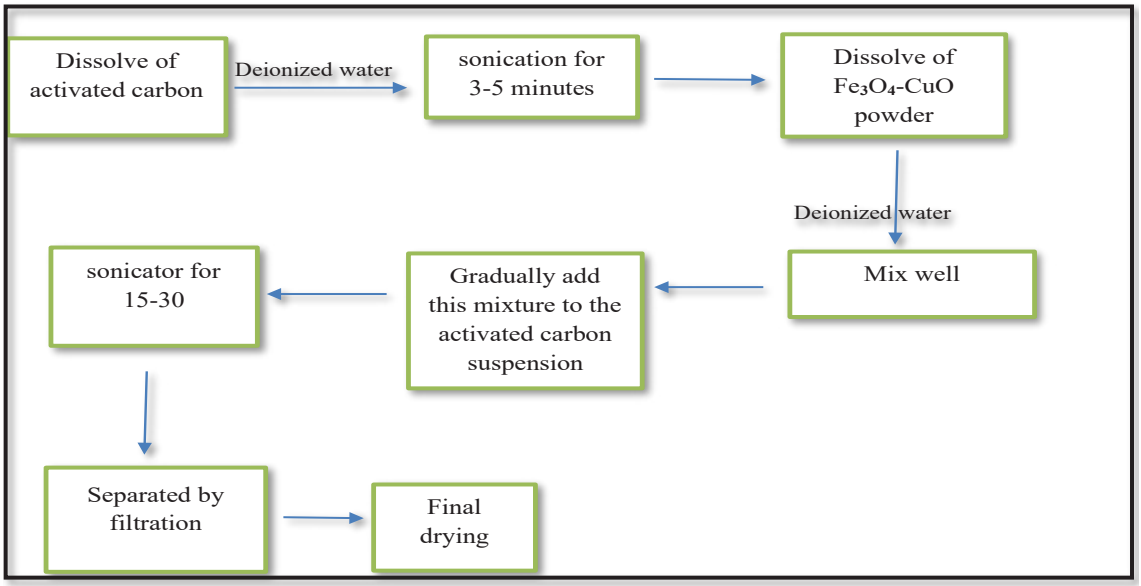

Fig. 5. Flowchart of synthesis Fe_3O_4-CuO NPS loaded for Activated Carbon.

aliphatic hydroxyl functional groups. The infrared spectrometry analysis of the surface of board at frequencies of 2922 cm^{-1} (C-H of the methyl group), 1735 cm^{-1} (C=O of the ester groups), 1648 cm^{-1} (C-C of the aromatic groups), 1527 cm^{-1} (C-N plastic vibration) indicates that carbon has more sites available for absorption, due to the presence of (C=C) aromatic groups which can be attributed to cellulose transforming into graphite-like carbon upon roasting [26]. The presence of low frequency bands in the finger area 500-600 cm^{-1} gives an indication of ash or silica contained in the crusts. Fig. 6 illustrates the comparative spectra between the Ac peach peels and indicates the presence of a

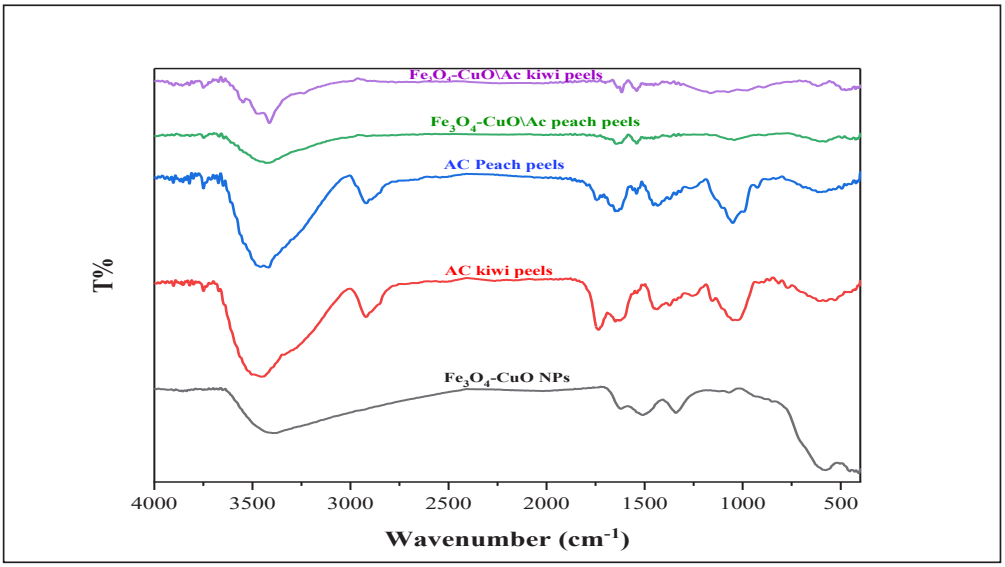

Fig. 6. FT-IR spectra of Fe_3O_4-CuO, Ac kiwi peels, Ac Peach peels, Fe_3O_4-cuO\Ac peach peels, Fe_3O_4-CuO\Ac kiwi peels nanoparticles.

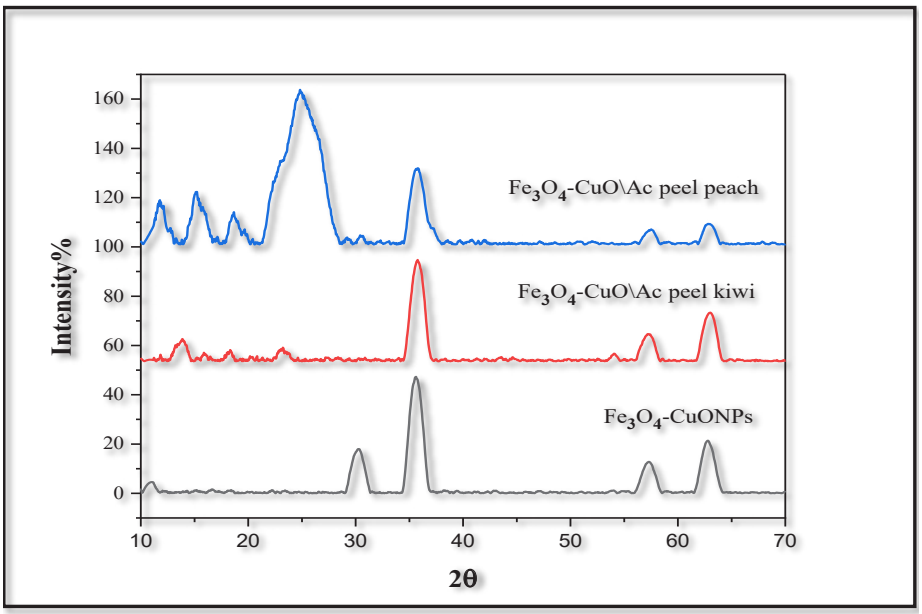

Fig. 7. XRD analysis of (Fe_3O_4-CuO) nanoparticles, Fe_3O_4-CuO\Ac kiwi peel, Fe_3O_4-CuO\Ac peach peel.

broad band, representing the hydroxyl O-H group (3458/3415 cm^{-1}) which is characteristic of plant peels [27]. Broad, weak bands are observed in the 1103-1049 cm^{-1} region that can be attributed to hydroxyl groups. Several bands were identified at the following frequencies: 2918 cm^{-1} (the C-H broad band of the methyl group), 1745 cm^{-1} (the carbonyl (C=O) group), 1668-1637 cm^{-1} (from the lignin network), 1527 cm^{-1} (the C=C (Non-aromatic) band), corresponding to (Ac) in the spectra and C-N vibrational group. The presence of these groups on the carbon surface prior to and after acid treatment can provide additional sites for sorption to occur. In addition to these, some weak vibrations (493-615 cm^{-1}) were detected and suggest the existence of ash/silica in crusts [28]. Another important characteristic in the Forth spectrum for the compound Fe_3O_4-CuO/Ac peach is that it displays 3414 cm^{-1} band, which can be associated with a broad band due to O-H hydroxyl groups. Such bands are typically seen for plant peels. Significant broad bands seen at around 1043 cm^{-1} suggest the presence of alcohol functional groups. A series of bands seen at 1643 cm^{-1} are due to the broad C=C aromatic group present in Ac and are representative of the C–N vibrational group, which is an indicator of additional sites for adsorption on the carbon surface prior to and post acid treatment. The formation of aromatic C=C groups as a result of transforming the configurations of cellulose during the roasting process has also aided in increasing the aromatic character of the carbon structure. In addition, weak bands ranging from 422–611 cm^{-1} have also been observed as evidence of Fe–O and Cu-O stretching vibrations in the Fe_3O_4 and CuO compounds, respectively. The FTIR spectrum of the kiwi compound Fe_3O_4–CuO/Ac also demonstrates a broad absorption between 3400-3500 cm^{-1}, characteristic of an O-H hydroxyl group. In this spectrum, weak, broad peaks from 1161–1074 cm^{-1} may also be indicative of the presence of alcohol functional groups. The presence of bands at 1637-1616 cm^{-1} and at 1541 cm^{-1} indicates that the Ac compound has an aromatic C=C group [31] and a C–N vibrational functional group. This implies that these C=C groups will yield a carbon framework with an increased aromatic character due to the rearrangement of the cellulose structure upon being roasted. Slight vibrations (observed in the range 472–617 cm^{-1}) were observed and assigned to the stretching modes of Fe–O and Cu–O bonds in the CuO and Fe_3O_4 materials, respectively [32].

XRD analysis

Fig. 7 below shows the X-ray diffraction (XRD)

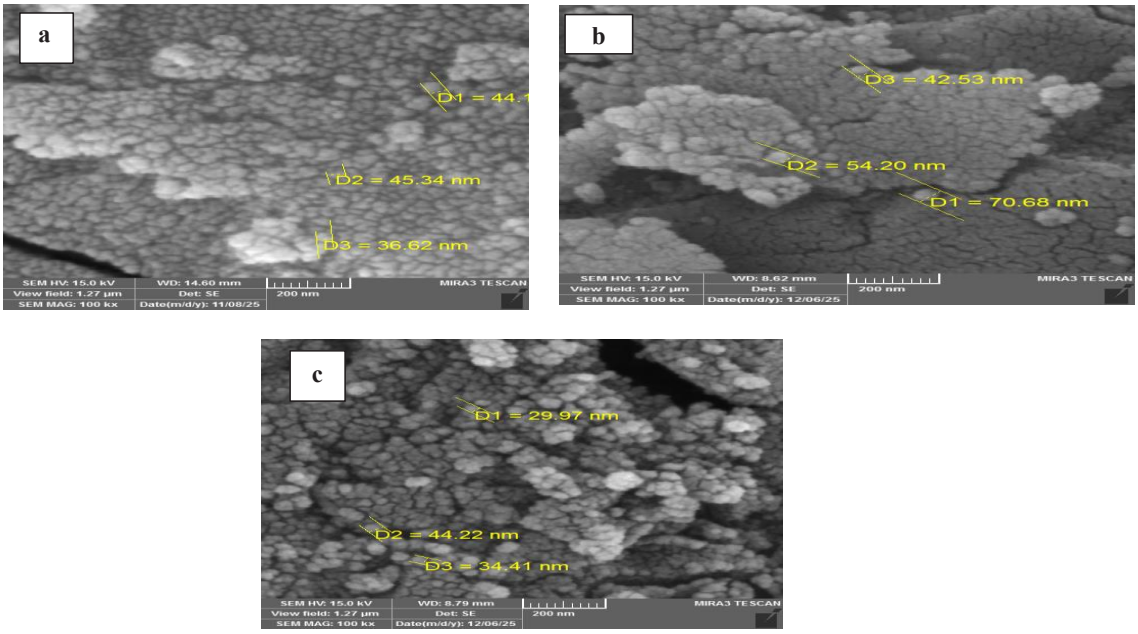

Fig. 8. SEM images of (a) Fe_3O_4-CuO nanoparticles, (b) Fe_3O_4-CuO/Ac of peel kiwi nanoparticles, (c) Fe_3O_4-CuO/Ac of peel peach nanoparticles.

planes CuO, Fe_3O_4 and nanoparticles produced from the Cu Kα radiation (λ = 1.54 Å) with conditions of 40 Kv and 30 mA. The observed peaks produced peaks (220), (311), (511), (440) at distinct angles of 30.25°,35.62°, 57.28° and 62.78° respectively. This means that the Fe_3O_4 nanoparticles were formed in a pure monoclinic structure and did not contain any impurities either from the synthesis process or any prior processes (reference JCPDS card number 88-0866) [33]. The best example of a (311) peak is also seen in the literature at the overlapping peak shared between Fe_3O_4 and CuO, which is at an angle of 35.62°. Additionally, there were many more diffraction peaks observed at (220) as well as were observed corresponding to the CuO phase at the (220) crystal planes from (220) diffraction reflected as well [34]. Since these peaks were not present when comparing the diffraction peaks in the Fe_3O_4 to the diffraction peaks of CuO, it can be concluded that the Fe_3O_4-CuO nanocomposite was synthesized. Since the XRD analysis showed clear-cut, distinct and sharp diffraction patterns for all the 44-CuO and 44-Fe_3O_4 nanoparticles, this indicates that they are made up of polycrystalline structures with a crystal size of 3.9 nm, as determined by the Scherrer Equation [35].

Scanning Electron Microscope and Energy Dispersive X-Ray Analysis (SEM& EDX)

The nanoparticles of the Nanoscale dimensions of 200 nm (Fig. 8a) display a homogeneous nanostructure of the Fe_3O_4-CuO compound in which the Fe_3O_4-CuO has been formed as nanoscale spherical and distributed nanoparticles due to magnetic and intermolecular attractions between them. The Fe_3O_4-CuO particles' diameters were from (36-45) nm across. These results corroborate the previous work(s) estimation of the incomplete formation of the Fe_3O_4-CuO composite nanoparticles, which generally have an approximate size range of 25-60 nm (36). Additionally, the surface texture of this nanocomposite indicates the materials have an increased surface roughness (i.e. are rough) therefore enhancing adsorption and catalysis performance due to large surface area. The Fig. 8b image, showing combined and/or irregularly shaped, clustered will indicate that the Fe_3O_4-CuO is distributed on the surface of the activated carbon, resulting in increased active surface area with additional sites for adsorption as compared to activated carbon alone. Fruit peel-derived activated carbon is formed by an activation method that produces a small-to-medium-sized pore structure at the surface. Previous studies support this finding [37]. There are nanoparticles in close proximity to the carbon surface with a size of 30-45 nm (Fig. 8c); these dimensions fall within the range of 1-100 nm, thereby optimizing their available area for surface interactions. It is

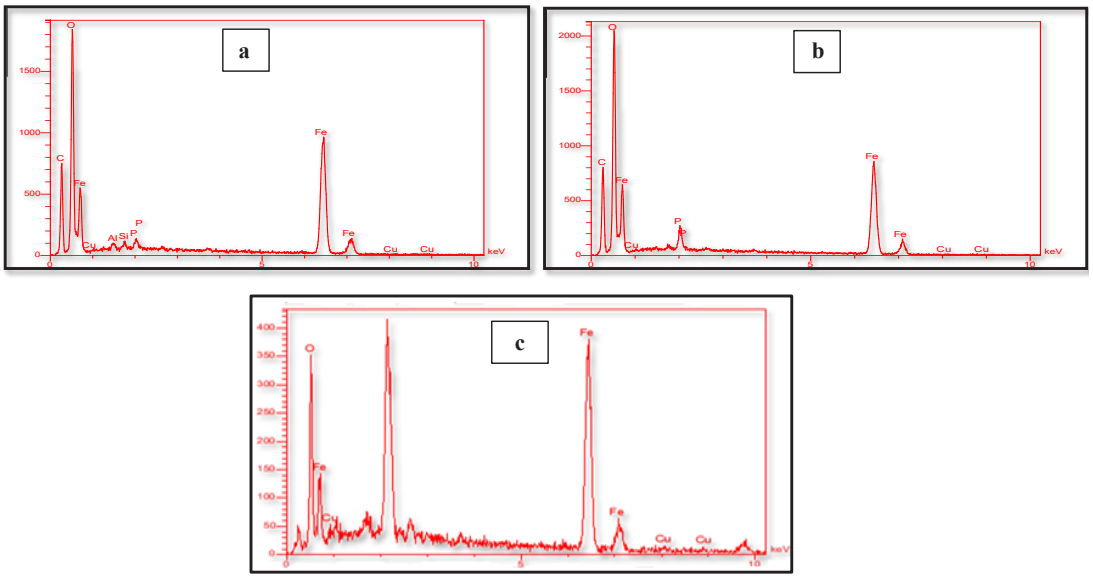

Fig. 9. EDX spectra of (a) Fe_3O_4-CuO nanoparticles, (b) Fe_3O_4-CuO/Ac of peel kiwi nanoparticles, (c) Fe_3O_4-CuO/Ac of peel peach nanoparticles.

evident from the data that both Fe_3O_4 and CuO nucleate and adhere to the activated carbon surface, creating additional pore-like structures and thus increasing the number of effective reaction sites (interconnected porous networks). SEM images illustrate that the activated carbon is either deposited or "loaded onto" the Fe_3O_4-CuO composite material within the report. Some researchers have suggested that activated carbon produced from fruit/vegetable sources typically

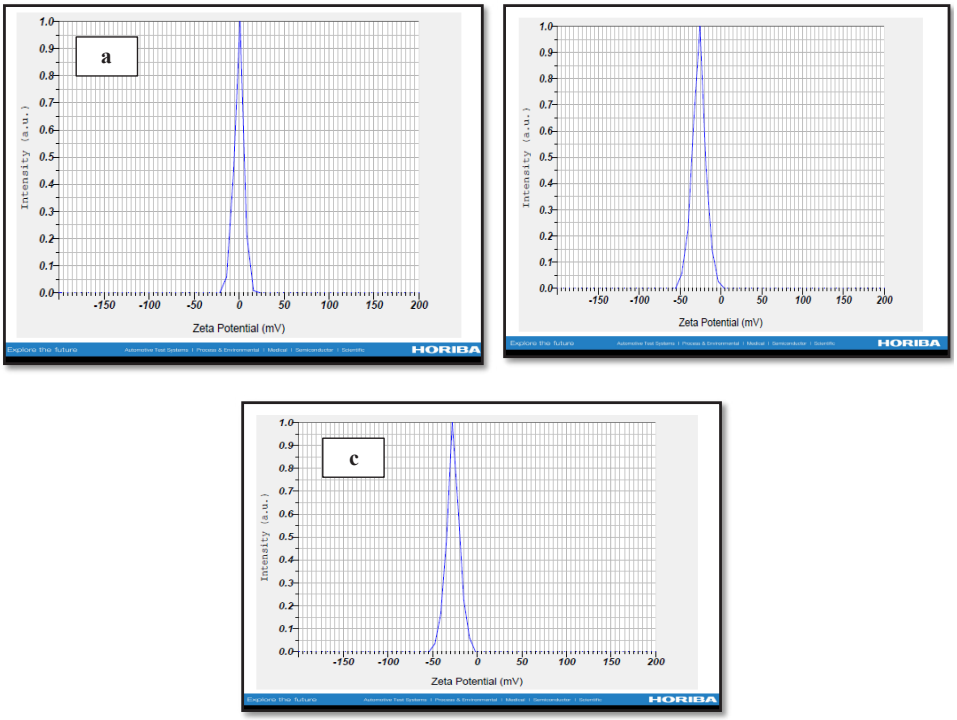

Fig. 10. Zeta potential spectra (a) Fe_3O_4-CuO nanoparticles of Fe_3O_4-CuO nanoparticles, (b) Fe_3O_4-CuO/Ac of peel kiwi nanoparticles, (C) Fe_3O_4-CuO/Ac of peel peach nanoparticles.

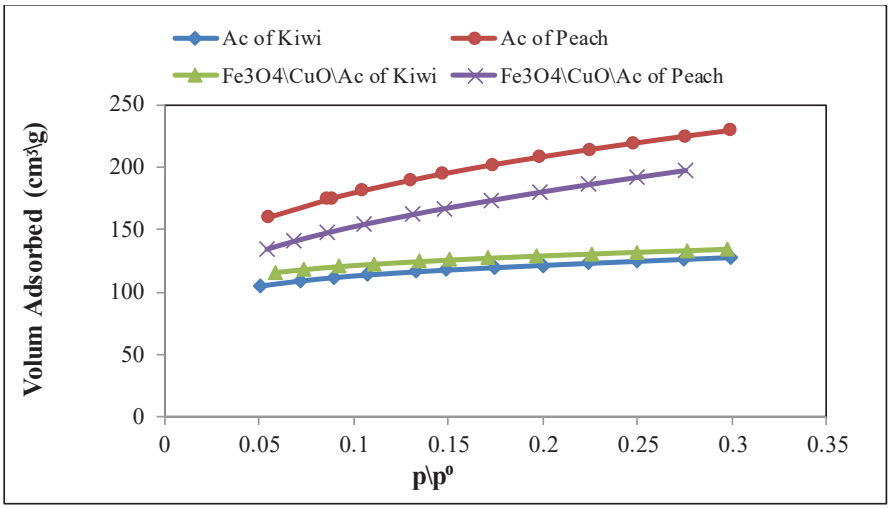

Fig. 11. BET surface of Ac of peel kiwi,Ac of peel peach, Fe_3O_4/CuO/Ac of peel kiwi, Fe_3O_4/CuO/Ac of peel peach.

exhibits a relatively high level of porosity, resulting in an increased number of available active surface reaction site densities [38].

The EDX analysis of the Fe_3O_4-CuO nanocomposite provided the results illustrated by Fig. 9a; Fig. 9a showed that active carbon was formed as the base material from the analysis is approximately 80.47% (Fe), 17.11% (O), and 2.41% (Cu) by weight with the atomic percentages being approximately 41.97%, 56.54%, and 1.49% corresponding to iron, oxygen and copper respectively, which closely resembles results from previous studies ([39]). The peaks for each of the elements listed (C, Fe & Cu) were all evident (Fig. 9b) indicate that both the Fe_3O_4 and CuO were combined together on the surface of the carbon matrix during preparation and subsequent storage. The EDX spectra produced from the present investigation is in line with similar EDX results in earlier studies as well ([38]). As seen in Fig. 9, both the substrate shows evidence of iron (Fe) and carbon (C) through a successful ferric oxide (Fe(III)) reduction reaction to produce copper (Cu) from cupric oxide (CuO). Evidence of oxygen (O) was detected combining with the metal oxide. The presence of these elements illustrates efficient loading of the nanocomposite onto the activated carbon surface [40].

Zeta potential

The zeta potential (λ) is the potential energy associated with the movement of ions and colloids due to the applied electric field; it is a measurement of the surface charge used to provide information on suspension stability via zeta potential measurements. Particles that exhibit near-neutral zeta potentials or mildly charged surfaces will have a negligible amount of charge at an average of approximately (-0.4 mV) as illustrated in Fig. 10a indicating no net charge is present on the surface of the Fe_3O_4-CuO compound. This low surface charge indicates that this compound is only weakly held together by electrostatic forces. However, when 0.1% PEG is used at dilute concentrations, it forms a vacuum barrier at the surface of the particles, thereby providing effective stability against particle aggregation by providing steric hindrance—a

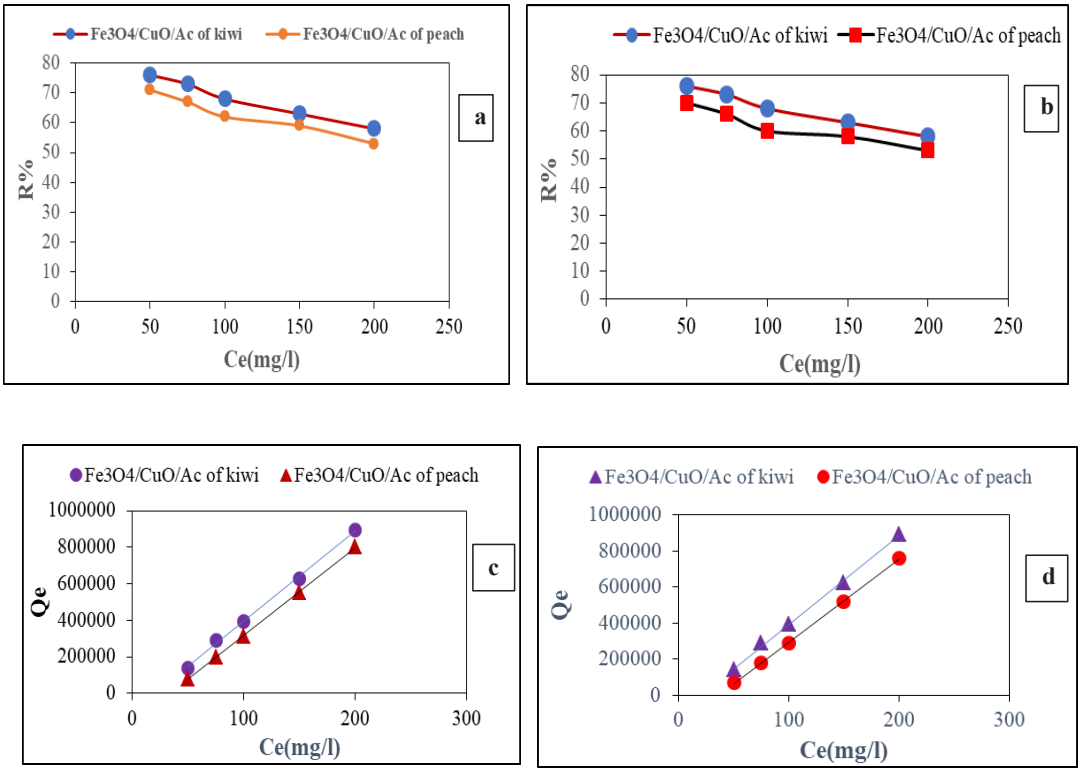

Fig. 12. Effect of Intial concentration of (a,c) Fe_3O_4/CuO/Ac of kiwi of Crystal violet , and (b,d) Fe_3O_4/CuO/Ac of peach of Erichrom black T.

well-established method of providing stability to ionic systems using nonionic polymers—thereby significantly enhancing the stability of the Fe 3 O 4 -CuO system as compared to both the control and 1.0% PEG (0.2% w/v) systems. Zeta Measurement conducted on Kiwi Peel created AC/ Fe_3O_4-CuO composites yielded a negative surface potential of -27 mV at room temperature 25 degrees Celsius (°C) as depicted in Fig. 10b. This indicates that the surfaces are negatively charged due to the ionization of functional groups such as COOH and -OH. The moderate to good colloidal stabilities suggest that sufficient electrostatic repulsive forces exist to prevent agglomeration of the particles which enhances the adsorption of cationic dyes because of the electrostatic attraction between the negatively charged particles and the positively charged dye molecules. The uniform peak distributions also support the homogeneity of the surface charge and the success of the loading process [42]. Based on zeta potential measurements as shown in Fig. 10c (three separate measurements); the generated combination of Fe_3O_4/CuO (2:1, by weight) provided an average zeta potential value of - 26.8 mV, which is attributed to the negatively charged oxygen functional groups along the carbon surface. This measurement also highlights the exceptional cationic dye absorption capacity of the Fe_3O_4/CuO combination with the associated contribution from the iron and copper oxides [43].

BET surface

Micropores and semi-pores constitute the majority of activated carbon's (from kiwi peel) ability to adsorb contaminants using

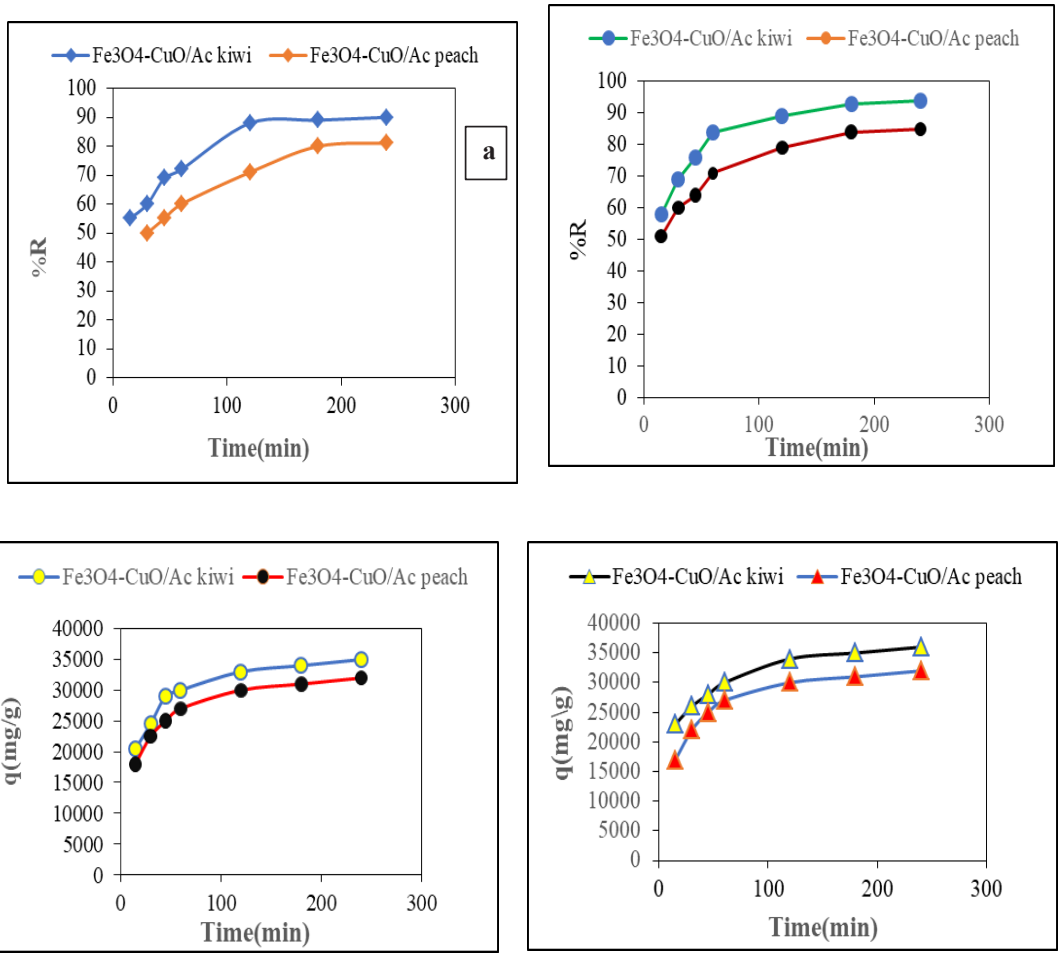

Fig. 13. Effect of Equilibrium time of (a,c) Fe_3O_4/CuO/Ac of kiwi of Crystal violet , and (b,d) Fe_3O_4/CuO/Ac of peach of Erichrom black T.

the adsorption mechanism. When plotting an adsorption isotherm in Fig. 11 using a BET analysis, activated carbon's adsorption curve will demonstrate a consistent and gradual rise with increasing P/P°; thus, indicating that most of the adsorption process for activated carbon will occur within the micropore region [44]. Peach peel contains chemical compounds that, when converted to activated carbon, result in an increase in both the total number of pores and the total surface area of the activated carbon (compared to activated carbon derived from kiwi peel). In addition, the BET adsorption isotherm for peach peel-based activated carbon will demonstrate the highest cumulative N2 (number of moles per unit volume) adsorbed at every P/P° point, indicating a substantially higher pore volume density than the activated carbon derived from kiwi peel. Moreover, the addition of metal oxides, such as Fe_3O_4 & CuO, will slightly reduce the surface area of activated carbon, as determined by BET, compared to the surface area of activated carbon that has not been loaded with the respective oxide(s). Iron oxide(s) and copper oxide(s) may occlude some of the micropores created within the activated carbon material. When activated carbon is loaded with oxide materials, effective pore size will decrease for early adsorption due to the emergence of the metal oxide(s), while resulting in a potential increase in chemisorption on the oxide surfaces [45]. The addition of metals to the PEACH AC significantly decreased the surface area compared to the unloaded PEACH AC, however it still had significantly greater surface areas than both the

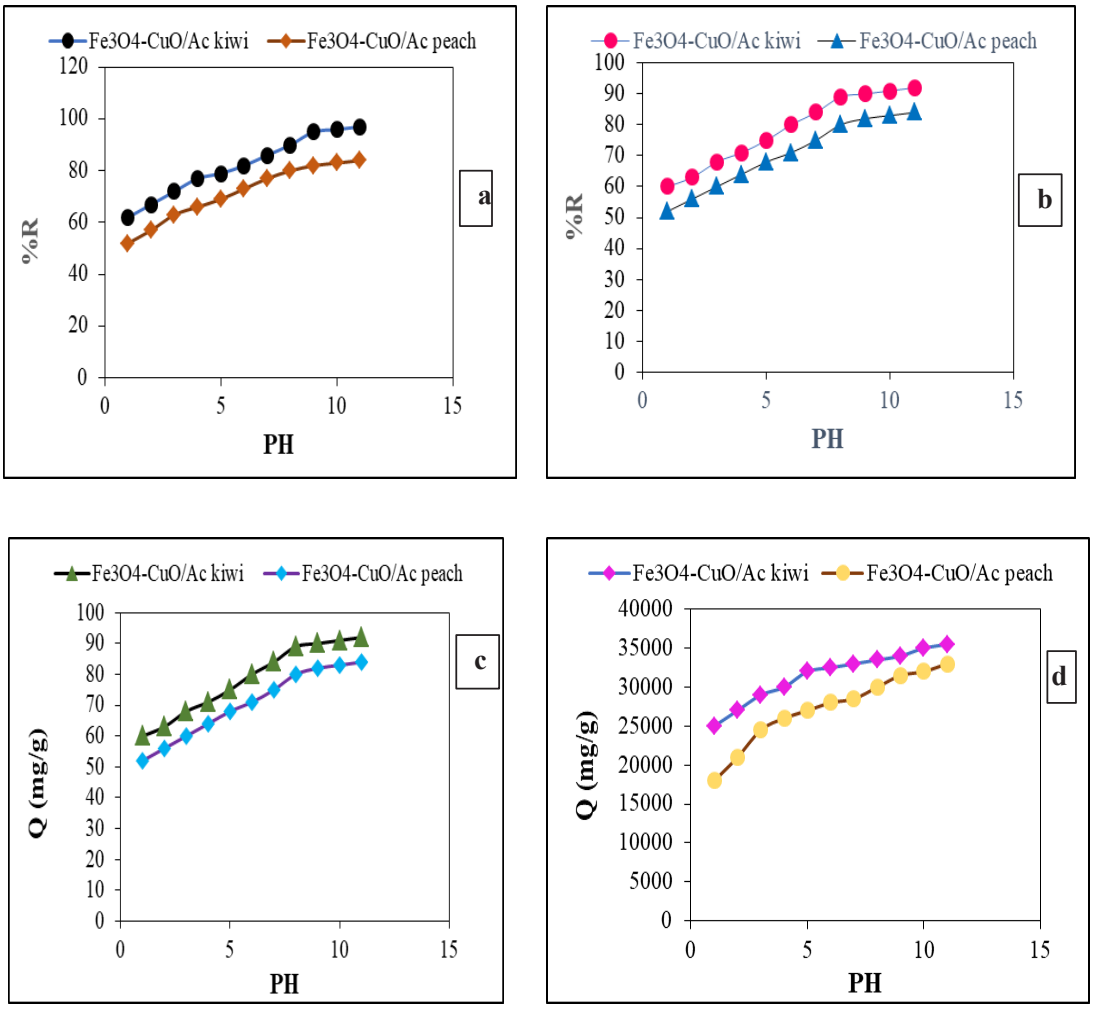

Fig. 14. Effect of PH of (a,c) Fe_3O_4/CuO/Ac of kiwi of Crystal violet , and (b,d) Fe_3O_4/CuO/Ac of peach of Erichrom black T.

KIWI AC and the LOADED KIWI AC. The height of the static adsorption curve for LOADED PEACH AC was greater than the three other samples. Furthermore, as the original PEACH AC has a large amount of surface area, the loading of the metal oxides (Fe_3O_4/CuO) will still have a relatively high surface area because it is based on a larger starting point. [46].

Adsorbtion

Intial of Concentration

The removal percentage (R%) falls at high concentrations because of the scarcity of active sites and the occurrence of surface saturation, whereas the adsorption capacity (qe) rises with growing initial concentration because of the increased driving force for the pollutant transfer towards the surface of the activated carbon, Fe_3O_4, and CuO as shown in Fig. 12. This behavior is in line with reports found in published works on magnetic nanocomposites and activated carbon [51].

Effiect of equilibrium time

Adsorption of molecules and ions occurs on vacant areas of the activated carbon surface, and as time increases, the amount of molecules and ions adsorbed by adsorption on activated carbon reduces the concentration difference between the surface of the activated carbon and the solution; therefore, decreasing the adsorption rate of the solids to the activated carbon. The initial stage of the adsorption process has high rates, but will be approaching equilibrium, where no more solids can be absorbed by activated carbon. Adsorption at the beginning of contact has high rates due to the high number of vacancies, and after time, vacancies become fewer and fewer, the rate

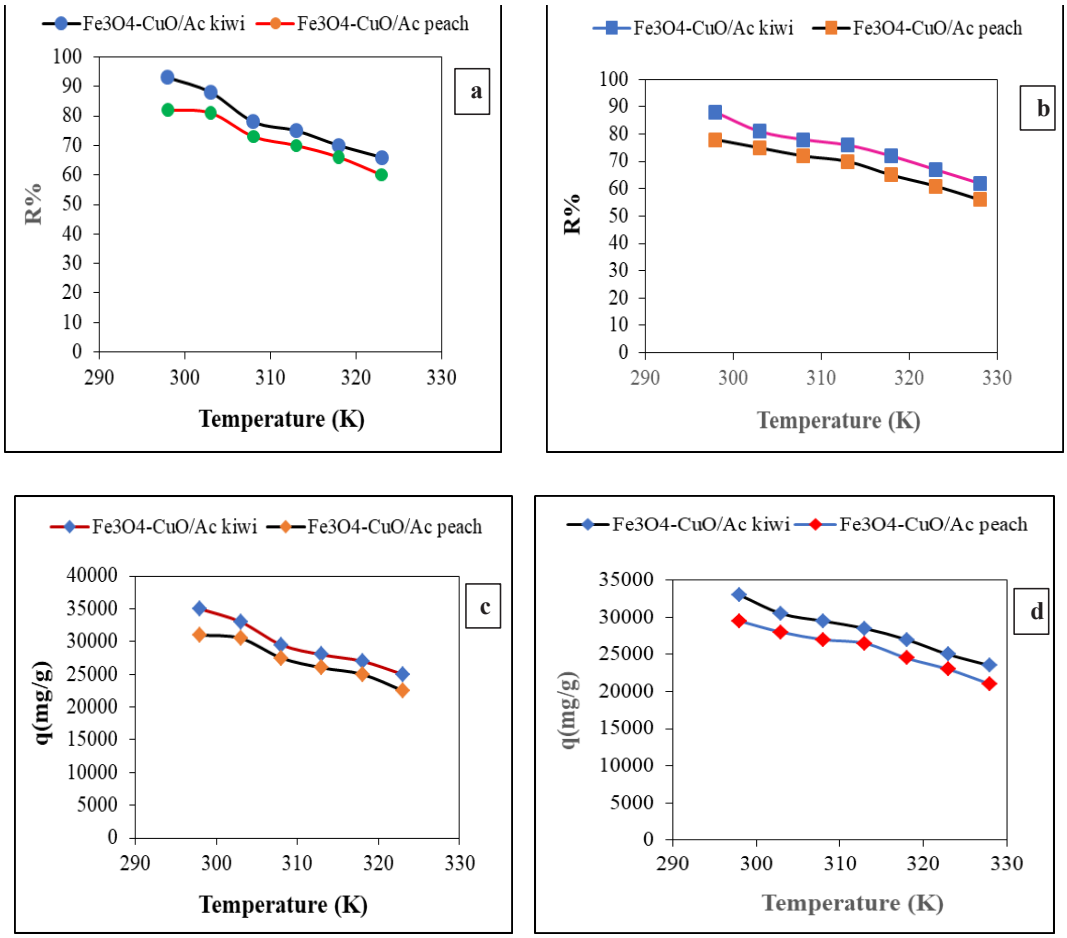

Fig. 15. Effect of Temperature of (a, c) Fe_3O_4/CuO/Ac of kiwi of Crystal violet, and (b, d) Fe_3O_4/CuO/Ac of peach of Eriochrome black T.

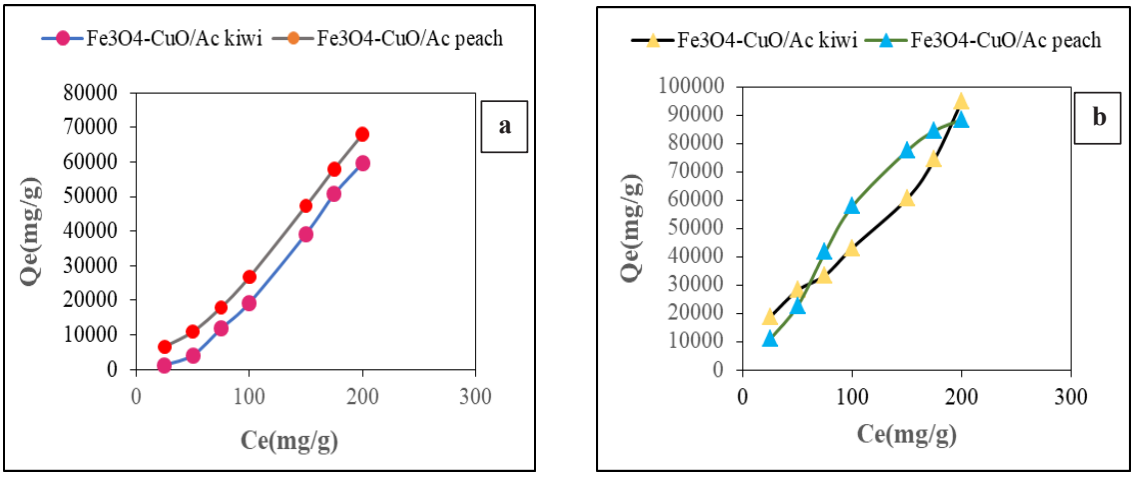

Fig. 16. The percentage of the surface of the mixture Fe_3O_4-CuO/Ac of kiwi and peach at a temperature of 25C°, pH 3 and the initial concentration 75 mg/ L, on (a) EBT, (b) CV.

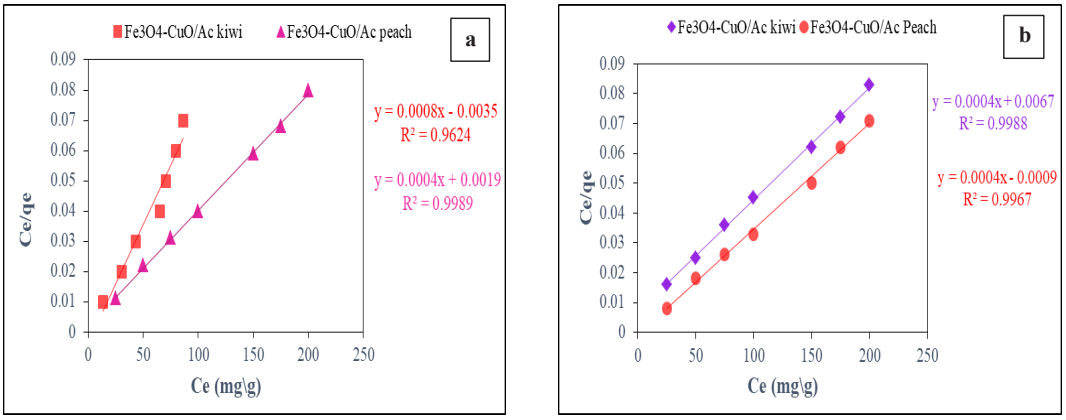

Fig. 17. Langmuir isotherm for adsorption of the mixture (Fe_3O_4-CuO/Ac of kiwi and peach) a temperature of 25C, pH 3 and the initial concentration 75 mg/ L on (a) EBT (b) CV.

Table .1. Langmuir and Freundlich constants for Crystal violet, Eriochrome black T, on the surface of the mixture (Fe_3O_4-CuO/Ac of peel kiwi and peel peach).

Dyes	Surface	Langmuir equation			Freundlich equation		
		KL	Q max	R^2	KF	1/n	R^2
Crystal violet	Fe_3O_4-CuO/Ac of peel kiwi	4.38	283.7	0.9624	71.862	1.7	0.9931
	Fe_3O_4-CuO/Ac of peel peach	5.3	188.7	0.9989	225.11	1.8	0.9906
Eriochrome black T	Fe_3O_4-CuO/Ac of peel kiwi	4.75	526.3	0.9988	367.3	1.3	0.9628
	Fe_3O_4-CuO/Ac of peel peach	6.25	400	0.9967	204.3	1.2	0.9886

of the reaction will become slower, and after reaching equilibrium, the amount of adsorption on activated carbon does not continue to increase, as demonstrated in Fig. 13.

Effiect of PH

The pH will influence the type and charge of the molecules or ions within the solution at different pH levels, depending on the pH of the adsorbent and its surface. The electrostatic attraction between the solute and the adsorbent surface will determine whether the adsorbent surface is negatively or positively charged as the pH increases to certain limits. When Qe reaches its maximum near the equilibrium pH, the charge on the adsorbent surface will be opposite to the charge of the solute molecules in solution. This would result in a higher removal %R of solutes at a pH that will enhance the attraction between the adsorbents surface and the solute to be removed

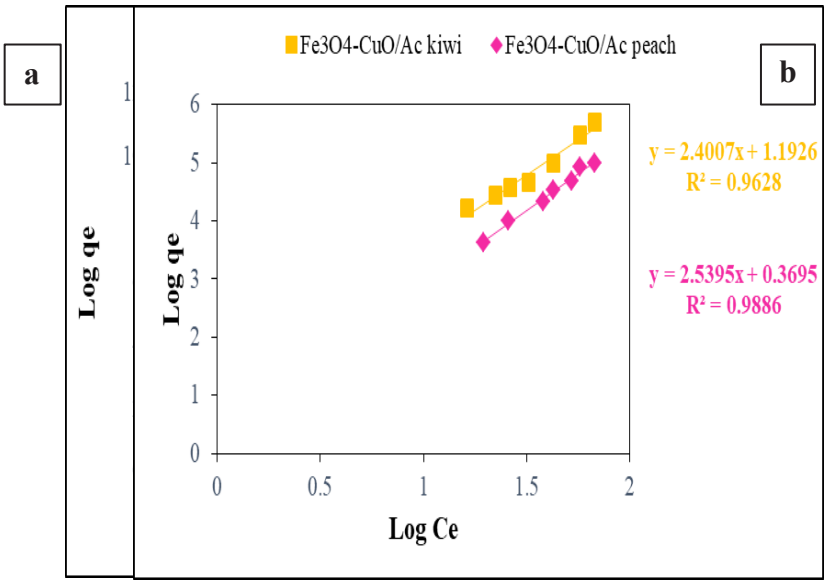

Fig. 18. The Freundlich isotherm for adsorption of the mixture (Fe_3O_4-CuO/Ac of kiwi and peach) at a temperature of 25C, pH 3 and the initial concentration 75 mg/ L on (a) EBT (b) CV.

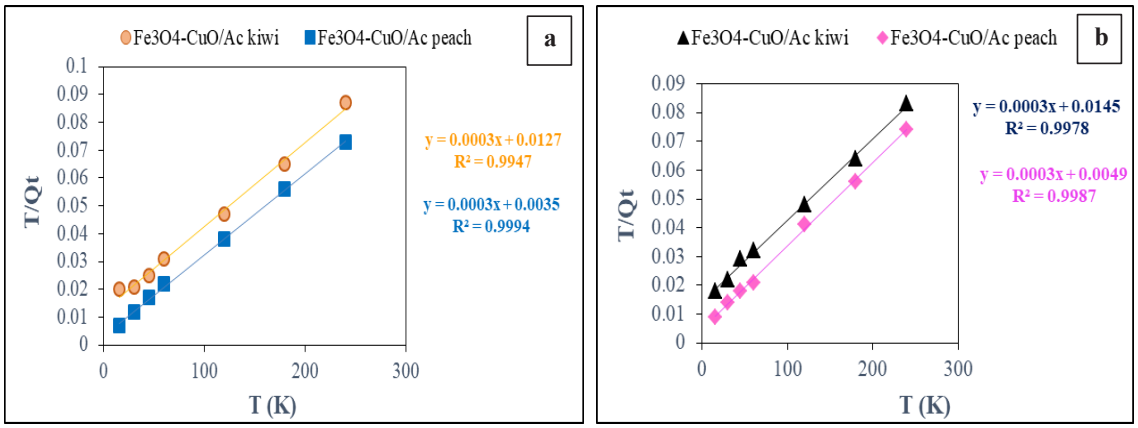

Fig .19. Pseudo-Order of (a) (Fe_3O_4-CuO) nanoparticles Fe_3O_4-CuO\Ac kiwi peel, Fe_3O_4-CuO\Ac peach peel in Crystal violete, (b) Fe_3O_4-CuO\Ac kiwi peel, Fe_3O_4-CuO\Ac peach peel in Eriochrome black T.

[48], as shown in Fig. 14.

Effect of temperture

The temperature has a significant impact on controlling the adsorption equilibria on nanosurfaces because it directly affects the kinetic energy of all molecules, and as the temperature increases, it also increases the likelihood of molecular collisions with the adsorbent's surface. Conversely, increasing the temperature may also enhance the pore size (therefore, increasing pore permeability) and aid in the diffusion of molecules through the pores, thus raising Qe; however, in some instances, the adsorption process is endothermic, while in others, the adsorption process is exothermic, and therefore, increasing the temperature causes an inhibition of the reaction and a subsequent decline in both Qe and R% (Fig. 15).

Adsorption Isotherm

The adsorption of carbon produced using kiwi and peach peels to the surface of an Fe_3O_4-CuO nanocomposite was studied using 0.01 g (Fe_3O_4-CuO) in a 50 mL solution, pH 3 for EBT dye, pH 9 for CV dye, and contact times of 120 s for Crystal Violet dye and 180 s for Aero chrome Black T dye, at 25 °C (Fig. 16a, b). The correlations of Ce with Ce/Qe indicated good agreement with the Langmuir model on both of these surfaces (Fig. 17a, b). The relationships ofLnCe vs Ln Qe were consistent with the Freundlich model (Fig. 18a, b). The Freundlich equation represents the adsorption characteristics of heterogeneous surfaces, the adsorption of heterogeneous materials, and multi-layer and different energy adsorption [50]. Based on these results, it was concluded that the adsorption processes on the Fe_3O_4-CuO-activated carbon composite conformed to both the Langmuir and Freundlich models. According to the results, there is an excellent match between experimental data from both the Langmuir and Freundlich Models of Adsorption, with a particularly good fit with the Langmuir Model due to its one-layer adsorption of adsorbates directly onto Fe_3O_4 and CuO molecules. This implies the presence of relatively homogeneously distributed adsorption sites on the external surfaces of the materials being studied [51]. Thus, this confirms that the materials are homogeneous with respect to their single-layer surface adsorption capabilities. The data for the Freundlich Model indicates that the materials contain heterogeneous surfaces and therefore also provide for the possibility of multilayer adsorption because of the wide variety of pore sizes and functional groups that comprise the activated carbon structure (Fig. 18). Therefore, the agreement between these models provides evidence that the surfaces contain both a combination of homogeneously and heterogeneously distributed sites; this is very typical behavior for most nanomaterials [52]. RL represents the shape of the adsorption curve and defines whether the system exhibits favorable, unfavorable or irreversible adsorption ($R^2 < 0$). The Table 1 shows the statistical results of the following variables: Q max; KL; KF; R^2 for each of the curves created from plotting the surface adsorption of carbon (activated) on the (Fe_3O_4 – CuO) (surface) by the produced adsorbents (prepared adsorptions) [53].

Pseudo-Order

The results in Fig. 19 show that the second-order model is the most suitable to describe the adsorption process compared to the first-order archetypal, because the R coefficients of the second model are much higher. This reflects that the reaction sites on the surface of the nanocomposite are the main determinant of the rate and absorption, and not just the concentration of the substance [54]. The predicted values for adsorption capacity (qe) were closer to experimental values than the first-order model. This implies that the surface adsorption mechanism has a bigger impact on the reaction rate, and that the rate-limiting step includes either a chemical reaction or an electron exchange between the surface sites of the nanoparticle or the adsorbent (Fig.19a,b) [55].

CONCLUSION

Based on the results obtained, it can be confirmed that preparing activated carbon from kiwi and peach peels and loading it onto the surface of the Fe_3O_4-CuO nanocomposite led to the formation of a composite material, and the Fe_3O_4 and CuO nanoparticles enhanced the surface activity as a result of the harmonious effect between the metallic and carbon phases. The advanced porous structure and high specific surface area contributed to increasing the number of active sites available for adsorption and had advanced physical and chemical properties.

The results also showed:

1. The adsorption mechanism is due to the interaction of several reactions, such as electron exchange between the pollutant and the surface, electrostatic attraction, and hydrogen bonds.

2. The adsorption capacity (Qe) and removal percentage (%R) were high compared to unloaded carbon.

3. That the adsorption process was mostly chemical the kinetic data followed a pseudo-second-order model, indicating.

4. This indicates the formation of a monolayer of adsorbed molecules at relatively homogeneous sites, where the equilibrium data agree with the Langmuir model.

5. Where the results also agree with the Freundlich model. This indicates a heterogenous surface and multilayer adsorption at some sites.

6. Where the surface combines homogeneous and heterogeneous regions, this dual conformity and complex surface structure reflect the incorporation of metallic nanoparticles with porous carbon.

7. The magnetic properties of the composite facilitated the maintenance of high efficiency during reuse cycles in the separation and extraction process after adsorption. Therefore, activated carbon loaded onto the Fe_3O_4-CuO composite is a promising material with characterized by good stability and high adsorption performance. practical applications in efficient and economical industrial water treatment.

CONFLICT OF INTEREST

The authors declare that there is no conflict of interests regarding the publication of this manuscript.

REFERENCES

1. Sontakke SS, Rupwate AS, Baile M, Jain A. Removal of dye by using activated charcoal prepared by kitchen waste. Journal of Pharmaceutical and Biological Sciences. 2021;9(2):123-126.
2. Lin J, Ye W, Xie M, Seo DH, Luo J, Wan Y, et al. Environmental impacts and remediation of dye-containing wastewater. Nature Reviews Earth and Environment. 2023;4(11):785-803.
3. Khatri Z, Ahmed F, Khatri A, Khatri M, Qureshi UA, Kim I-S. Screen-printed electrospun cellulose nanofibers using reactive dyes. Cellulose. 2017;24(10):4561-4568.
4. Rathi BS, Kumar PS, Vo D-VN. Critical review on hazardous pollutants in water environment: Occurrence, monitoring, fate, removal technologies and risk assessment. Sci Total Environ. 2021;797:149134.
5. Holkar CR, Jadhav AJ, Pinjari DV, Mahamuni NM, Pandit AB. A critical review on textile wastewater treatments: Possible approaches. J Environ Manage. 2016;182:351-366.
6. Kaykhaii M, Sasani M, Marghzari S. Removal of Dyes from the Environment by Adsorption Process. Chemical and Materials Engineering. 2018;6(2):31-35.
7. Rápó E, Tonk S. Factors Affecting Synthetic Dye Adsorption; Desorption Studies: A Review of Results from the Last Five Years (2017–2021). Molecules. 2021;26(17):5419.
8. Arellano-Cárdenas S, López-Cortez S, Cornejo-Mazón M, Mares-Gutiérrez JC. Study of malachite green adsorption by organically modified clay using a batch method. Appl Surf Sci. 2013;280:74-78.
9. Yilmaz E, Soylak M. Functionalized nanomaterials for sample preparation methods. Handbook of Nanomaterials in Analytical Chemistry: Elsevier; 2020. p. 375-413. http://dx.doi.org/10.1016/b978-0-12-816699-4.00015-3
10. Karimi-Maleh H, Kumar BG, Rajendran S, Qin J, Vadivel S, Durgalakshmi D, et al. Tuning of metal oxides photocatalytic performance using Ag nanoparticles integration. J Mol Liq. 2020;314:113588.
11. Ahmadi M, Elmongy H, Madrakian T, Abdel-Rehim M. Nanomaterials as sorbents for sample preparation in bioanalysis: A review. Anal Chim Acta. 2017;958:1-21.
12. Khan WA, Arain MB, Soylak M. Nanomaterials-based solid phase extraction and solid phase microextraction for heavy metals food toxicity. Food and Chemical Toxicology. 2020;145:111704.
13. Liu W-X, Song S, Ye M-L, Zhu Y, Zhao Y-G, Lu Y. Nanomaterials with Excellent Adsorption Characteristics for Sample Pretreatment: A Review. Nanomaterials. 2022;12(11):1845.
14. Masoud MS, Haggag SS, Heiba HF, Abd El-Hamed OH, Habila NS, Abdel-hamid IAM, et al. Comparative Adsorption Affinities of Nano-Metal Oxides Towards Cr(VI): Synthesis, Characterization, Kinetics, Isotherms, Thermodynamic and Techno-Economics Study. Environmental Processes. 2023;10(2).
15. Gheju M, Balcu I, Mosoarca G. Removal of Cr(VI) from aqueous solutions by adsorption on MnO 2. J Hazard Mater. 2016;310:270-277.
16. Krishna Kumar AS, Jiang S-J, Warchoł JK. Synthesis and Characterization of Two-Dimensional Transition Metal Dichalcogenide Magnetic MoS_2@ Fe_3O_4 Nanoparticles for Adsorption of Cr(VI)/Cr(III). ACS Omega. 2017;2(9):6187-6200.
17. Kumar KY, Raj TNV, Archana S, Prasad SBB, Olivera S, Muralidhara HB. SnO2 nanoparticles as effective adsorbents for the removal of cadmium and lead from aqueous solution: Adsorption mechanism and kinetic studies. Journal of Water Process Engineering. 2016;13:44-52.
18. Rejani P, Radhakrishnan A, Beena B. Adsorption of Pb(II) on Nano Sized SnO2 Derived from Sol-Gel Method. International Journal of Chemical Engineering and Applications. 2014;5(3):244-248.
19. Abid W, Ammar E. Date Palm (Phoenix dactylifera L.) Wastes Valorization: A Circular Economy Approach. Mediterranean Fruits Bio-wastes: Springer International Publishing; 2022. p. 403-430. http://dx.doi.org/10.1007/978-3-030-84436-3_17
20. Wang Y, Zhao G, Zhang G, Zhang Y, Wang H, Cao W, et al. An electrochemical aptasensor based on gold-modified MoS2/rGO nanocomposite and gold-palladium-modified Fe-MOFs for sensitive detection of lead ions. Sensors Actuators B: Chem. 2020;319:128313.
21. Thi Huong N, Thi Mai Huong P, Thi Kim Giang N, Thi Lan P, Thanh Dong V, Tien Dung C. Fe_3O_4/CuO/Chitosan Nanocomposites: An Ultrasound-Assisted Green Approach for Antibacterial and Photocatalytic Properties. ACS Omega. 2023;8(45):42429-42439.
22. Cameu GM, Almeida L, Oliveira AP, Igansi A, Jaeschke DP, Silveira N, et al. Enhanced Adsorption of Pb(II) and Cd(II) by Activated Carbon Derived from Peach Stones for Efficient Water Decontamination. Processes. 2025;13(10):3064.
23. Yang ZW, Fan X, Guo LA, Wei WT. Graphene Oxide/Fe_3O_4

Composites Prepared via In Situ Precipitation. Advanced Materials Research. 2014;904:150-154.
24. Kalaivani P, Mathubala G. Biosynthesis of CuO Nanoparticles using Coleus Aromaticus Leaf Extract for Efficient Catalytic Applications. Oriental Journal Of Chemistry. 2024;40(5):1320--1328.
25. Sim LC, Wong JL, Hak CH, Tai JY, Leong KH, Saravanan P. Sugarcane juice derived carbon dot–graphitic carbon nitride composites for bisphenol A degradation under sunlight irradiation. Beilstein Journal of Nanotechnology. 2018;9:353-363.
26. Gubitosa J, Rizzi V, Fini P, Nuzzo S, Cosma P. Kiwi peel waste as a recyclable adsorbent to remove textile dyes from water: Direct Blue 78 removal and recovery. Physical Chemistry Chemical Physics. 2024;26(13):9891-9905.
27. Bakti AI, Gareso PL. Characterization of Active Carbon Prepared from Coconuts Shells using FTIR, XRD and SEM Techniques. Jurnal Ilmiah Pendidikan Fisika Al-Biruni. 2018;7(1):33.
28. Tolkou AK, Maroulas KN, Theologis D, Katsoyiannis IA, Kyzas GZ. Comparison of Modified Peels: Natural Peels or Peels-Based Activated Carbons for the Removal of Several Pollutants Found in Wastewaters. C. 2024;10(1):22.
29. Nandiyanto ABD, Ragadhita R, Fiandini M. Interpretation of Fourier Transform Infrared Spectra (FTIR): A Practical Approach in the Polymer/Plastic Thermal Decomposition. Indonesian Journal of Science and Technology. 2022;8(1):113-126.
30. Lesiak B, Rangam N, Jiricek P, Gordeev I, Tóth J, Kövér L, et al. Surface Study of Fe_3O_4 Nanoparticles Functionalized With Biocompatible Adsorbed Molecules. Frontiers in Chemistry. 2019;7.
31. Allwar A, Ahdiaty R, Doong R. MAGNETIC Fe_3O_4-CuO/BIOCHAR Nanocomposite for Adsorption of Inorganic Anions from Aqueous Solution. RASAYAN Journal of Chemistry. 2022;15(04):2466-2476.
32. Yunus ZM, Othman N, Hamdan R, Ruslan NN. CHARACTERIZATION OF PHOSPHORIC ACID IMPREGNATED ACTIVATED CARBON PRODUCED FROM HONEYDEW PEEL. Jurnal Teknologi. 2015;76(5).
33. Dwivedi P, Malik A, Fatima Hussain HZ, Jatrana I, Imtiyaz K, Rizvi MMA, et al. Eco-Friendly CuO/Fe_3O_4 Nanocomposite synthesis, characterization, and cytotoxicity study. Heliyon. 2024;10(6):e27787.
34. Kaya MT, Calimli MH, Nas MS. Degradation of methylene blue with a novel Fe_3O_4/Mn_3O_4/CuO nanomaterial under sonocatalytic conditions. Res Chem Intermed. 2023;49(6):2549-2568.
35. Mariam Refka J, Nisha PA. A Study on Green Synthesis and Characterization of Silver Nanoparticles using Aloe Vera gel extract and Abelmoschus esculentus (Lady's Finger) extract and Its Antibacterial activity. South Asian Journal of Experimental Biology. 2024;14(1):31-35.
36. Mahmoodi NM, Taghizadeh M, Taghizadeh A. Mesoporous activated carbons of low-cost agricultural bio-wastes with high adsorption capacity: Preparation and artificial neural network modeling of dye removal from single and multicomponent (binary and ternary) systems. J Mol Liq. 2018;269:217-228.
37. Smagulova G, Imash A, Baltabay A, Keneshbekova A, Abdisattar A, Kazhdanbekov R, et al. Mechanistic Evaluation of Pb(II) Adsorption on Magnetic Activated Carbon/Fe_3O_4 Composites: Influence of Hydrothermal and Ultrasonic Synthesis Routes. C. 2025;11(4):83.
38. Londoño-Calderón CL, Tancredi P, Menchaca-Nal S, Francois NJ, Pampillo LG. Synergistic effects in magnetically recoverable nanocomposites of CuO nanoleaves with Fe_3O_4 nanoparticles for organic dye degradation. Next Materials. 2025;7:100370.
39. Sharma M, Sharma K, Kumar D, Gill FS, Ichikawa T, Jain A, et al. Process analysis of aqueous ciprofloxacin adsorption by biochar–magnetite nanocomposites. Discover Applied Sciences. 2025;7(10).
40. Allwar A, Shopiar SP, Wibawanti HP, Abimanyu RF, Maulina R, Indriyani N. Isotherms and kinetic studies of phenol and chlorophenol removal in aqueous solution by magnetic Fe_3O_4-CuO/biochar. AIP Conference Proceedings: AIP Publishing; 2022. p. 030030.
41. Khoshsang H, Ghaffarinejad A, Kazemi H, Wang Y, Arandiyan H. One-pot synthesis of S-doped Fe2O3/C magnetic nanocomposite as an adsorbent for anionic dye removal: equilibrium and kinetic studies. Journal of Nanostructure in Chemistry. 2017;8(1):23-32.
42. Kędzierska M, Potemski P, Drabczyk A, Kudłacik-Kramarczyk S, Głąb M, Grabowska B, et al. The Synthesis Methodology of PEGylated Fe_3O_4@Ag Nanoparticles Supported by Their Physicochemical Evaluation. Molecules. 2021;26(6):1744.
43. Janani B, Al-Mohaimeed AM, Raju LL, Al Farraj DA, Thomas AM, Khan SS. Synthesis and characterizations of hybrid PEG-Fe_3O_4 nanoparticles for the efficient adsorptive removal of dye and antibacterial, and antibiofilm applications. Journal of Environmental Health Science and Engineering. 2021;19(1):389-400.
44. Pochapski DJ, Carvalho dos Santos C, Leite GW, Pulcinelli SH, Santilli CV. Zeta Potential and Colloidal Stability Predictions for Inorganic Nanoparticle Dispersions: Effects of Experimental Conditions and Electrokinetic Models on the Interpretation of Results. Langmuir. 2021;37(45):13379-13389.
45. Wang B, Lan J, Bo C, Gong B, Ou J. Adsorption of heavy metal onto biomass-derived activated carbon: review. RSC Advances. 2023;13(7):4275-4302.
46. Harabi S, Guiza S, Álvarez-Montero A, Gómez-Avilés A, Bagané M, Belver C, et al. Adsorption of Pesticides on Activated Carbons from Peach Stones. Processes. 2024;12(1):238.
47. Zandi A, Abbastabar Ahangar H, Saffar A. Optimization removal of methylene blue from aqueous solution by adsorption on Fe_3O_4@PVA/GT magnetic nanocomposite by Taguchi method. Inorg Chem Commun. 2023;158:111528.
48. Farahmandzadeh F, Molahosseini E, Kermanshahian K, Molaei M, Nejadshafiee V. Fe_3O_4/activated carbon/EDTA magnetic nanocomposite: A high-performance and cost-efficient nano adsorbent for treatment of water from heavy metal ions and organic dyes. Diamond Relat Mater. 2025;159:112751.
49. Paneru KR, Jha BK. Adsorptive removal of Pb(II) ions from aqueous solution by activated carbon prepared from cabbage waste. Nepal Journal of Environmental Science. 2020;8:1-10.
50. Nurhilal O, Bagaskara A, Sihite AH, Hidayat S, Setianto S. Absorbance study on the adsorptive removal of Fe(III) ions using activated carbon from coconut shells. Current Research in Green and Sustainable Chemistry. 2025;10:100458.
51. Yang X, Wan Y, Zheng Y, He F, Yu Z, Huang J, et al. Surface functional groups of carbon-based adsorbents and their roles in the removal of heavy metals from aqueous solutions: A critical review. Chem Eng J. 2019;366:608-621.
52. Fisli A, Safitri RD, Nurhasni N, Dewi SH, Deswita D. Isotherm, Kinetics and Thermodynamics Adsorption Studies of Dye onto Fe_3O_4-Waste Paper Activated Carbon Composites. Jurnal Teknologi. 2020;83(1):45-55.
53. Topal Canbaz G. Fe_3O_4@Granite: A Novel Magnetic Adsorbent for Dye Adsorption. Processes. 2023;11(9):2681.
54. Acta Technica Corviniensis – Bulletin of Engineering.
55. Lv Y, Han S, Wen W, Bai X, Sun Q, Chen L, et al. Preparation of EDTA-2Na- Fe_3O_4-Activated Carbon Composite and Its Adsorption Performance for Typical Heavy Metals. Separations. 2025;12(8):205.